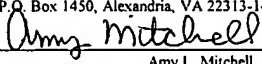


| | |
|---|------------------|
| Certificate of Mailing by "Express Mail" | |
| Mailing Label Number: | EL966273636US |
| Date of Deposit: | January 21, 2004 |
| I hereby certify that this paper or fee is being deposited with the United States Postal Service "Express Mail Post Office Box Addressee" service under 35 CFR 1.10 on the date indicated above and is addressed to the Commissioner for Patents, P.O. Box 1450, Alexandria, VA 22313-1450. | |
|  Amy L. Mitchell | |

In Vivo Raman Endoscopic Probe And Methods Of Use

Inventor: Haishan Zeng, citizen and resident of Canada

CROSS-REFERENCE

This application claims priority from provisional application No. 60/441,566, filed on January 21, 2003.

BACKGROUND OF THE INVENTION

Lung cancer is the leading cause of death from cancer in North America, and it has the second most common cancer incidence among both men and women. One in 11 Canadian men will develop lung cancer, and 1 in 12 will die from this condition, while one in 19 Canadian women will develop lung cancer, and 1 in 22 will die from this disease. Lung cancer also results in the most lost years of life due to cancer death in both men and women. The best outcome of lung cancer treatment is achieved when the lesion is discovered in the pre-invasive stage, which is also commonly referred as carcinoma in situ (CIS).

Early and accurate diagnosis of lung cancer offers a better chance of cure, results in the use of less radical treatment methods, and reduces the cost of treatment. The five-year survival for all stages of lung cancer is only 11-14 percent, while for Stage I it is 42 to 47 percent. Under optimal conditions, survival can be even higher. However, with respect to currently available lung imaging techniques, lung cancer is generally asymptomatic until it has reached an advanced stage, when the treatment outcome is poor. In particular, very early lung cancers are difficult to detect and localize by conventional white-light endoscopy since these cancers are only a few cell layers thick and up to a few millimeters in surface diameter, producing insufficient changes to make them visible under white light illumination. In the lung, only about 30 percent of CIS lesions are visible by conventional white-light bronchoscopy.

In the past decade, tissue autofluorescence imaging has been successfully used to improve the early detection of lung cancers. However, fluorescence endoscopy technology (developed at B.C. Cancer Agency and also referred as “LIFE” technology) has less optimal specificity for lung cancer detection (66 percent for LIFE compared to 90 percent for conventional white light bronchoscopy) although it improved the sensitivity from 25 percent for white light bronchoscope to 67 percent for LIFE. There is still much room for improvement in the diagnostic accuracy.

Recently, we have performed Raman spectroscopy measurements on fresh biopsy bronchial tissue samples and found significant spectral differences between normal and malignant lung tissues, demonstrating the potential of Raman spectroscopy for *in vivo* lung cancer detection.

In contrast to fluorescence technology, Laser-Raman spectroscopy probes molecular vibrations and gives very specific, fingerprint-like spectral features and has high accuracy for differentiation of malignant tissues from benign tissues. Raman spectroscopy can also be used to identify the structural and compositional differences on proteins and genetic materials between malignant lung cancers, their pre-cursors, and normal lung tissues. This knowledge will lead to better understanding, on the biochemical bases, of the evolution process of lung cancers from benign to malignancy. The biochemical information obtained from *in vivo* Raman measurements may also be helpful for predicting the malignancy potential of pre-invasive and invasive lung cancers. The objective of this invention is to develop a miniaturized laser-Raman probe, which can go through the instrument channel of a bronchoscope to perform Raman spectroscopy measurements of the bronchial tree *in vivo*. A further objective is to enable the application of Raman spectroscopy for *in vivo* lung cancer detection and evaluation, therefore, improve the specificity of lung cancer detection and the overall detection accuracy when combined with fluorescence endoscopy technology.

When monochromatic light strikes a sample, almost all the observed light is scattered elastically (Rayleigh scattering) with no change in energy (or frequency). A very small portion of the scattered light, about 1 in 10^8 , is inelastically scattered (Raman scattering) with a corresponding change in frequency. The difference between the incident and scattered frequencies corresponds to an excitation of the molecular system, most often excitation of vibrational modes. By measuring the intensity of the scattered photons as a function of the frequency difference, a Raman spectrum is obtained. Raman peaks are typically narrow (a few wavenumbers) and in many cases can be attributed to the vibration of specific chemical bonds (or normal mode

dominated by the vibration of a single functional group) in a molecule. As such, it is a “fingerprint” for the presence of various molecular species and can be used for both qualitative identification and quantitative determination.

In recent years, Raman spectroscopy has been investigated for *in vitro* diagnosis of malignancies in various organs (e.g., brain, breast, bladder, colon, larynx, cervix, and skin). These studies show that features of tissue Raman spectra can be related to the molecular and structural changes associated with neoplastic transformations. A sensitivity and specificity of 82 percent and 92 percent respectively for differentiating between cervical precancerous and other tissues *in vitro* have been reported. Mahadevan-Jansen, *Raman spectroscopy for the detection of cancers and precancers*, *J BIOMED. OPT.* 1, 31-70, 1996.

In vivo NIR Raman measurements have also been reported in the cervix, colon, esophagus, and the skin. Mahadevan-Jansen, *Development of a fiber optic probe to measure NIR Raman spectra of cervical tissue in vivo*, *PHOTOCHEM. PHOTOBIOLOG.* 68: 427-431, 1998; Shim, *In vivo near-infrared Raman spectroscopy: demonstration of feasibility during clinical gastrointestinal endoscopy*, *PHOTOCHEM. PHOTOBIOLOG.* 72: 146-150, 2000; Huang, *Rapid near-infrared Raman spectroscopy system for real-time in vivo skin measurements*, *OPT. LETT.* 26: 1782-1784, 2001; Utzinger, *Near-infrared Raman spectroscopy for in vivo detection of cervical precancers*, *APPL. SPECTROSC.* 55:955-959, 2001.

Shim *et al.* have shown differences for *in vivo* Raman spectra among normal, precancerous, and cancerous esophageal and gastric tissues. Raman spectroscopy of lung tissues, however, has only been reported on formalin-fixed parenchyma lung diseases, which provide very limited guidance to *in vivo* applications due to the adverse effect of formalin fixation on tissue Raman spectra. Kaminaka, *Near-infrared Raman spectroscopy of human lung tissues: possibility of molecular-level cancer diagnosis*, J. RAMAN SPECTROSC. 32:139-141, 2001; Kaminaka, *Near-infrared multichannel Raman spectroscopy toward real-time in vivo cancer diagnosis*, J. RAMAN SPECTROSC. 33:498–502, 2002; Shim, *The effects of ex vivo handling procedures on the near-infrared Raman spectra of normal mammalian tissues*, PHOTOCHEM. PHOTOBIO. 63: 662-671, 1996.

The development of an *in vivo* tissue Raman probe is technically challenging due to the weak Raman signal of tissue, interference from tissue fluorescence and spectral contamination caused by the background Raman and fluorescence signals generated in the fiber itself. Most probes published in literature and commercial products are larger than 10 mm in diameter, and therefore are not suitable for endoscopy applications. The instrument channel of commonly-used bronchoscopes are 2.2 mm (for example, Olympus BF-20, BF-40).

To date, the only endoscopic probe utilized for *in vivo* measurements is the Enviva Raman probe manufactured by Visionex, Inc., Atlanta, GA. However, the company was dissolved two years ago; therefore, the probe is no longer commercially available. That probe consisted of a central delivery fiber (400 μm core diameter) surrounded by seven collection fibers (300 μm core diameter). It incorporated LP filters in the collection fibers and a BP filter in the delivery fiber.

The main disadvantages of that probe are that (1) only seven collection fibers were used, which cannot fill the full vertical height of the CCD sensor in the spectrometer; therefore, it was unable to gain the maximum sensitivity; and (2) the size of the collection fibers was big (300 μm), leading to poor spectral resolution ($> 20 \text{ cm}^{-1}$).

BRIEF SUMMARY OF THE INVENTION

The present invention comprises a novel endoscopic Raman probe. In the preferred embodiment, the probe comprises 58 collection fibers (100 μm core diameter), which will fill the CCD full vertical height and achieve spectral resolution of 8 cm^{-1} . However, a probe comprising a smaller or larger number of collection fibers will be appropriate for use with a spectrometer having a different sized CCD. The novel probe will also preserve the round-to-parabolic linear array configuration of the Raman probe for *in vivo* skin measurements, as described in United States Patent No. 6,486,948. The probe of the present invention therefore, will achieve similar superior S/N ratios and a short integration time of a few seconds or sub-seconds for each Raman spectral measurement.

The present invention utilizes the state-of-art fiber optic technology, filtering technology, laser machining technology, and the existing rapid Raman spectroscopy system, to build a miniaturized laser-Raman probe for use in an endoscope. In the preferred embodiment, the probe will pass through the instrument channel of a bronchoscope and acquire Raman spectra from the bronchial tree *in vivo*. In other embodiments, the probe will be used with other endoscopes. In other embodiments, the laser-Raman probe will be integrated with a

spectrometer to perform Raman spectroscopy for analysis of the *in vivo* tissue under examination.

The preferred embodiment of the invention comprises:

1. A special probing fiber bundle assembly of about 65 cm long and 1.9 mm in diameter to pass through the endoscope instrument channel and to be in contact with the tissue to provide illumination and to collect Raman scattering photons;
2. Special coatings applied to the distal end of the probing fiber bundle assembly to produce a short-pass (SP) filter on the single illumination fiber and a long-pass (LP) filter on the collection fiber bundle;
3. A novel filter adapter to accommodate a high quality band-pass (BP) filter to pass through only the laser light transmitted through the illumination fiber and also to accommodate a notch filter to block the back-scattered laser light from passing through the collection fiber bundle;
4. A round-to-parabolic linear array fiber bundle using laser-machining technology to relay the collected Raman signal to the Raman spectrometer for spectral analysis. This special fiber bundle serves to correct the spectrograph image aberration and improve signal to noise (S/N) ratio;
5. Integration of the probing fiber bundle assembly, the filter adapter, the illumination fiber, and the round-to-parabolic linear array fiber bundle to form the endoscopic laser-Raman probe.

This embodiment can be used in an endoscope. In another embodiment, the invention comprises the probe described above used in conjunction with a spectrometer capable of performing Raman spectral analysis.

BRIEF DESCRIPTION OF DRAWINGS

The foregoing and other objects, features, and advantages of the invention will be apparent from the following descriptions of preferred embodiments and drawings illustrating principals of the invention and its uses.

Figure 1 is a schematic block diagram of the rapid Raman spectrometer system for *in vivo* skin measurements.

Figure 2 is a schematic block diagram of the probe of the rapid Raman spectrometer system of Figure 1.

Figure 3a is an image of a 100 μm slit on a CCD through a spectrograph, showing image aberration.

Figure 3b is an image of the same 100 μm slit on a CCD through a spectrograph as in Figure 3a, corrected compared to the image of Figure 3a.

Figure 4 is a graphical representation for the curve observed in Figure 3a.

Figure 5a is Raman spectra of healthy palm skin in three acquisition modes at a CCD exposure time of 0.05 seconds: spectrum a is from complete software binning mode; spectrum b is from combined hardware and software binning mode; and spectrum c is from complete hardware binning mode.

Figure 5b is Raman spectra of healthy palm skin in three acquisition modes at a CCD exposure time of 0.5 seconds: spectrum a is from complete software binning mode; spectrum b is from combined hardware and software binning mode; and spectrum c is from complete hardware binning mode.

Figure 6 is mean Raman spectra of normal and malignant (adenocarcinoma and squamous cell carcinoma) bronchial tissues.

Figure 7 is a graph of the scatter plot of the ratio of intensities of Raman spectra at 1445 cm^{-1} to that at 1655 cm^{-1} with respect to diagnosis.

Figure 8 is schematic diagram of the *in vivo* Raman endoscopic probe of the present invention.

DETAILED DESCRIPTION OF THE INVENTION

We have successfully built a rapid Raman spectroscopy system, which can obtain a Raman spectrum from *in vivo* skin in less than one second. This system is described and claimed in United States Patent No. 6,486,948, the disclosure of which is incorporated by reference. Figure 1 shows the block diagram of the system. It consists of an external cavity-stabilized diode laser 4 (785 nm, 300 mW; Model 8530, SDL), a transmissive imaging spectrograph 2 (HoloSpec-f/2.2-NIR, Kaiser), a NIR-optimized, back-illuminated, deep-depletion, CCD detector 20 (LN/CCD-1024EHRB, Princeton Instruments), and a specially-designed Raman probe 8. The laser 4 is coupled to the Raman probe 8 via a 200- μm core-diameter fiber 6. The CCD 20 consists of 1024 X 256 pixels (27 μm X 27 μm) and allowed vertical binning for improved detection

sensitivity. The whole system was packed onto a movable cart for outpatient clinical data acquisition.

This Raman probe 8 was designed to maximize the collection of tissue Raman signals while reducing the interference of Rayleigh scattered light, fiber fluorescence, and silica Raman signals. The probe 8 as illustrated in Figure 2 consisted of two arms. An illumination arm 6 incorporated a collimating lens 42, band-pass filter (785 ± 2.5 nm) 34, and focusing lens 24, delivering the laser light onto the skin surface 9 with a spot size of 3.5 mm. A collection arm 10 with collimating lens 15 and refocusing lens 17 and a holographic notch plus filter 30 (OD > 6.0 at 785 nm, Kaiser) was used for collecting Raman emissions. To enhance the detection of the inherently weak Raman signals, we packed as many fibers 44 into the fiber bundle 10 as allowed by the CCD height (6.9 mm). The fiber bundle 10 consists of 58×100 - μm fibers arranged in a circular shape at the input end 46 of the probe 8 and a linear array at the output end 48 which was connected to the spectrograph's entrance. Another 50- μm fiber was placed at the centre of the output linear array and split out of the bundle to terminate with a SMA connector for wavelength calibration. At the circular end 46 the fibers were packed into a 1.6 mm diameter area, which also defined the measurement spot size at the skin surface 9.

It is well known that the image of a straight slit through any spectrograph utilizing a plane grating has a curved line shape that is usually parabolic. This image aberration arises from the fact that rays from different positions along the length of the slit are incident on the grating at varying degrees of obliqueness. For spectrographs with short focal lengths, this obliqueness

causes significant distortion that can affect the measurement performance of the detector. Figure 3a shows the image aberration of a 100- μm slit through the spectrograph in an uncorrected system when illuminated by an Hg-Ar lamp. The curvature of the spectral lines is apparent, and in Figure 4 the horizontal displacement of a spectral line from Figure 3a is shown graphically with the displacement rounded to pixels (dashed line). The maximum horizontal displacement is five pixels (135 μm). The solid line is a linear regression-fitted parabolic curve described by

$$x=1.1904E-5y^2+1.9455E-4y-0.98613 \quad \text{Eq. 1}$$

where x is the horizontal displacement at a vertical position, y .

This image aberration causes two problems to hardware binning of CCD columns: (1) it decreases the spectral resolution; and (2) it decreases the S/N ratio achievable otherwise. It also causes problems with wavelength calibration. “Hardware binning” is CCD binning performed before signal read-out by the preamplifier. For signal levels that are readout noise limited such as for weak Raman signal measurements, hardware binning improves S/N linearly with the number of pixels grouped together. Binning can also be done using software after the signal is read out. However, “software binning” improves the S/N only by as much as the square root of the number of pixels added together. Hence, complete hardware binning of the entire vertical line is preferable for maximizing S/N. Prior to our work there has been no effort reported for correcting this image aberration. The manufacturer (Kaiser) of the HoloSpec spectrograph 2 of Figure 1, which was used in obtaining the spectra of Figure 3a, suggested binning the 11 segments shown in Figure 4 separately using hardware binning and then shifting the appropriate number of pixels before summing them together using software. We call this a “combined hardware and software binning procedure”. Another method is to acquire the whole image first

and then add all the pixels along the curved line together by software. We call this “complete software binning procedure.”

We conceived a simple but novel solution for dealing with this image aberration: a round-to-parabolic linear array. We aligned the 58×100-μm fibers of the fiber bundle 10 at the spectrograph end 48 along a curved line formed by laser drilling of a stainless steel cylinder piece, the shape of which directly corresponded to the horizontal displacement shown in Figure 4 but in the reverse orientation. Figure 3b shows the CCD image of the fiber bundle 10 illuminated by an Hg-Ar lamp. The central dark spots in the spectral lines are from the calibration fiber that was not illuminated. Using this specific fiber arrangement, the spectral lines are substantially straight, indicating effective image aberration correction that in turn allows us to completely bin the entire CCD vertical line (256 pixels) without losing resolution and reducing S/N. Therefore the S/N improvement we achieve with our system could be up to a maximum value of $11/\sqrt{11}=\sqrt{11}=3.3$ times when compared to the combined hardware and software binning procedure, and $256/\sqrt{256}=\sqrt{256}=16$ times compared to the complete software binning.

The *in vivo* skin Raman measurements using the ‘948 system under hardware binning mode can be obtained in less than 1 second, and some Raman peaks are discernible even with an exposure time of 0.01 seconds. The illumination power density is 1.56 W/cm², less than the ANSI maximum permissible skin exposure limit of 1.63 W/cm² for a 785-nm laser beam. A shutter was mounted at the laser output port and was synchronized with spectral data acquisition to make sure that the skin was only exposed to the laser light during the CCD exposure period.

Figures 5a and 5b shows Raman spectra from a palm at a CCD exposure time of 0.05 seconds (Figure 5a) and 0.5 seconds (Figure 5b). The spectra were obtained under complete software binning (spectra a and d), combined hardware and software binning (spectra b and e), and complete hardware binning (spectra c and f) acquisition modes. In both Figures 5a and 5b, the S/N ratios of the spectra using hardware binning are better than that of the combined hardware and software binning and are much better than that of complete software binning. Please note the Raman peak at 1745 cm^{-1} (from the C=O stretching band of lipid ester carbonyl) is barely visible on curve d, but appeared as a noisy small peak on curve e, whereas on curve f (obtained by our rapid Raman system) it appears as a smooth peak with great confidence.

Using the above rapid Raman system, we have measured Raman spectra on fresh normal and malignant lung tissue biopsies. The results demonstrated consistent spectral difference between normal and cancerous tissues. Figure 6 shows the mean Raman spectra of normal and malignant (adenocarcinoma and squamous cell carcinoma) bronchial tissues. Each of the Raman spectra was normalized to the integration area under the curve to correct for variations in absolute spectral intensity.

It can be seen that while significant Raman spectral differences exist between normal and tumor tissue, Raman spectra of adenocarcinoma are very similar to those of squamous cell carcinoma with slight differences in the relative intensities of the 1335 , 1445 and 1655 cm^{-1} bands. Primary Raman peaks at 752 , 823 , 855 , 876 , 935 , 1004 , 1078 , 1123 , 1152 , 1172 , 1208 , 1265 , 1302 , 1445 ,

1518, 1582, 1618, 1655, and 1745 cm^{-1} can be consistently observed in both normal and tumor tissues, with the strongest signals at 1265, 1302, 1445 and 1655 cm^{-1} . The intensities of Raman peaks at 855, 1078, 1265, 1302, 1445, and 1745 cm^{-1} in normal tissue are greater than those of tumor tissue, while Raman bands at 752, 1004, 1223, 1335 and 1550-1620 cm^{-1} are more intense in tumor tissue.

Besides the intensity differences between normal and tumor tissue, the spectral shape differences were also apparent in the 1000-1100, 1200-1400, and 1500-1700 cm^{-1} regions. Raman signals from 1200-1400 and 1500-1700 cm^{-1} were broader in tumor tissue as compared to normal tissue, and Raman peaks at 1322 and 1335 cm^{-1} were much enhanced in tumor tissue. In addition, the peak positions at 1078 and 1265 cm^{-1} in normal tissue appeared to have shifted to 1088 and 1260 cm^{-1} in tumor tissue, respectively.

Figure 7 shows the scatter plot of the ratio of intensities at 1445 cm^{-1} to that at 1655 cm^{-1} with respect to pathological results. One notes that the peak intensity at 1655 cm^{-1} is higher than that at 1445 cm^{-1} in tumor tissue. In contrast, the band intensity at 1445 cm^{-1} is stronger than that at 1655 cm^{-1} in normal tissue. The mean ratio value (1.25 ± 0.05 , $n=7$) of normal tissue is significantly different from the mean ratio value (0.77 ± 0.03 , $n=8$) of malignant tumor (adenocarcinoma+SCC) tissue (unpaired Student's t-test, $p < 0.0001$). The decision line ($I_{1445}/I_{1655}=1$) completely separates tumor tissue from normal tissue without any overlaps.

Assignment of the various Raman bands observed in Figure 6 is shown in Table 1. From these assignments, the measured Raman spectra suggest that lung tumors have increased nucleic acid, tryptophan, phenylalanine content and decreased phospholipids, proline, and valine content than normal tissue. Further analysis of these spectra also suggests that proteins in normal tissue are more in the α -helical confirmation, while in malignant tissue, some proteins were involved in the β -pleated sheet or random coil configurations. The results of these preliminary data indicate that NIR Raman spectroscopy provides a significant potential for the non-invasive diagnosis of lung cancers and warranty the development of an endoscopic Raman probe for *in vivo* applications.

Table 1. Peak positions and tentative assignments of major vibrational bands observed in normal and tumor bronchial tissue. Note: ν , stretching mode; ν_s , symmetric stretch; ν_{as} , asymmetric stretch; δ , bending mode; ν =very; s =strong; m =medium; w =weak; sh =shoulder.

| PEAK POSITION (cm^{-1}) | PROTEIN ASSIGNMENTS | LIPID ASSIGNMENTS | OTHERS |
|---------------------------------------|--|--|---|
| 1745w | | ν (C=O), phospholipids | |
| 1655vs | ν (C=O) amide I, α -helix, collagen, elastin | | |
| 1618s (sh) | ν (C=C), tryptophan | | ν (C=C), porphyrin |
| 1602ms (sh) | δ (C=C), phenylalanine | | |
| 1582ms (sh) | δ (C=C), phenylalanine | | |
| 1552ms (sh) | ν (C=C), tryptophan | | ν (C=C), porphyrin |
| 1518w | | | ν (C=C), carotenoid |
| 1445vs | δ (CH ₂), δ (CH ₃), collagen | δ (CH ₂) scissoring, phospholipids | |
| 1335s (sh) | CH ₃ CH ₂ wagging, collagen | | CH ₃ CH ₂ wagging nucleic acids |
| 1322s | CH ₃ CH ₂ twisting, collagen | | |
| 1302vs | δ (CH ₂) twisting, wagging, collagen | δ (CH ₂) twisting, wagging, phospholipids | |
| 1265s (sh) | ν (CN), δ (NH) amide III, α -helix, collagen, tryptophan | | |
| 1223mw (sh) | | | $\nu_{as}(\text{PO}_2^-)$, nucleic acids |
| 1208w (sh) | ν (C-C ₆ H ₅), tryptophan, phenylalanine | | |
| 1172vw | δ (C-H), tyrosine | | |
| 1152w | ν (C-N), proteins | | ν (C-C), carotenoid |
| 1123w | ν (C-N), proteins | | |
| 1078ms | | ν (C-C) or ν (C-O), | |

| | | phospholipids | |
|-------------|--|---------------|----------------|
| 1031mw (sh) | δ (C-H), phenylalanine | | |
| 1004ms | ν_s (C-C), symmetric ring breathing, phenylalanine | | |
| 963w | Unassigned | | |
| 935w | ν (C-C), α -helix, proline, valine | | |
| 876w (sh) | ν (C-C), hydroxyproline | | |
| 855ms | ν (C-C), proline | | Polysaccharide |
| | δ (CCH) ring breathing, tyrosine | | |
| 823w | out-of-plane ring breathing, tyrosine | | |
| 752w | symmetric breathing, tryptophan | | |

For successful *in vivo* Raman spectral measurement through the endoscope, the key specifications of the endoscopic laser-Raman probe are:

1. Be small enough to pass through the instrument channel (2.2 mm size) of the endoscope;
2. Incorporate proper filtering mechanism to minimize or eliminate the background Raman and fluorescence signals generated from the fiber-optic material; and
3. Be able to collect enough signal so that a Raman spectrum can be acquired in seconds or sub-seconds.

To preserve the high S/N ratio advantage of the skin Raman probe described in the '948 patent, the present invention utilizes a two-step filtering strategy for the endoscopic Raman probe: (1) first-order filtering at the tip of the fiber bundle and (2) high-performance filtering at the entrance point of the instrument channel of the endoscope.

Figure 8 shows the schematics of the preferred embodiment of the endoscopic Raman probe system 100 of the present invention. It consists of a probing fiber bundle assembly 110, a filter adapter 120, an illumination fiber 130, and a round-to-parabolic linear array fiber bundle 140. The illumination light from the diode laser 150 is focused into the illumination fiber 130, which is connected to the filter adapter 120 close to the entrance of the instrument channel of the bronchoscope 116. The illumination light is chosen to be at a wavelength as close as possible that will excite the molecules of interest. In the preferred embodiment, laser light at 785 nm meets this objective for detection of lung cancer. Other wavelengths can be chosen depending on the properties of the molecules of interest.

A high-performance BP filter (in the preferred embodiment, 785 ± 2.5 nm) 122 passes through the laser light and filters out the background Raman and fluorescence signals generated inside the illumination fiber 130 between the diode laser 150 and the filter adapter 120. The filtered laser light is refocused into the illumination fiber 132 in the probing fiber bundle assembly 110. Because this part of the illumination fiber 132 is short, the generated background Raman and fluorescence from the fiber is small. Nevertheless, the distal end 114 of the illumination fiber 132 is coated with a SP filter 160 to further reduce these background signals. The induced Raman signal from the tissue 170 is picked up by collection fibers 180 in the probing fiber bundle assembly 110. LP filter coatings 190 are applied to these fibers 180 to block the back-scattered laser light from entering the probe 110. At the proximal end 112 of the probing fiber bundle assembly 110, these collection fibers 180 are packed into a round bundle 184 and connected to the filter adapter 120. A notch filter (in the preferred embodiment, OD > 6.0 at 785 nm, Kaiser) 126 is used to further block the laser wavelengths and allow the Raman signals to

pass through. The Raman signals are refocused by a focusing lens 127 into the round-to-parabolic linear array fiber bundle 140. At the entrance of the spectrometer 152, these collection fibers 140 are aligned along a parabolic line 154 to correct for image aberration of the spectrograph to achieve better spectral resolution and higher S/N ratio in a fashion similar to the skin Raman probe described in the '948 patent.

To preserve the high S/N ratio advantage achieved in the skin Raman probe work described in the '948 patent, the probing fiber bundle assembly 110 of the preferred embodiment will consist of 58 100- μm collection fibers 180 and a 200- μm illumination fiber 132. These fibers are preferably low-OH fused silica type with N.A. = 0.22. The bifurcated assembly 110 has a diameter of 1.9 mm and a length of 65 cm to feed through the instrument channel of an endoscope 116, preferably an Olympus BF-20 or BF-40 bronchoscope. This assembly 110 is kept as short as possible to reduce background Raman and fluorescence signals from the fiber material. It is just about two cm longer than the length of the instrument channel.

At the distal common end 114, the illumination fiber 132 is located at the centre of the bundle 182 and its end is coated (such as coatings made by LightMatrix Technologies, Inc.) to generate a SP filter 160 with a cut-off wavelength, in the preferred embodiment, of around 825 nm. The collection fibers 180 are arranged around the illumination fiber 132 and their ends are coated to generate a LP filter 190 with a cut-off wavelength, in the preferred embodiment, of around 825 nm. Alternatively, more advanced technologies, e.g. fiber-Bragg gratings, may be used. At the proximal end 112, the assembly 110 is branched out into a single illumination fiber 132 and a collection fiber bundle 184 (circular shape) to be connected to the filter adapter 120. In the

assembly 110, the illumination fiber 132 is metal coated for optical isolation to prevent cross-talks with collection fibers 180.

The filter specifications described and utilized are dependent upon the laser wavelength used and are described for the preferred embodiment. Generally, if the laser wavelength is λ_0 , the BP filter should pass light of $\lambda_0 \pm \Delta\lambda$. The cut-off wavelength for LP and SP filters is $\lambda_0 + \Delta\lambda_1$. In the preferred embodiment, $\lambda_0 = 785$ nm, $\Delta\lambda = 2.5$ nm and $\Delta\lambda_1 = 40$ nm.

So, in the preferred embodiment, the BP filter 122 passes light between 782.5 and 787.5 nm, thereby isolating the illumination light from the laser 150 to the illumination fiber 132 at 785 nm. This illumination light then pass through a SP filter 160 with a cut-off of 825 nm, to pass light shorter than this wavelength and attenuate longer wavelengths, to further ensure that no illumination light exists in the signal range above 825 nm. The illumination light then encounters the subject 170 and induces Raman scattering. The Raman-scattered light enters the collection fibers 180 after first passing through the LP filter 190 with a cut-off of 825, pass light above this wavelength and attenuate shorter wavelengths, to ensure that no non-specific light, such as would result from reflection from the laser illumination light or non-Raman-scattered light, will enter the measurement system. The notch filter 126 then further ensures that no laser light proceeds into the spectrometer 152.

When performing endoscopic Raman measurements, the distal end 114 of the endoscope 116 is in gentle contact with the tissue surface 170. A quartz window 118 (or other materials with low

Raman and fluorescence background) may be attached to the end of the probe 116 to keep the probe 116 at a fixed distance from the tissue surface 170. When the probe 116 is moved away from the tissue surface 170, the sampling depth will change. Pulling the probe 116 away from the tissue surface 170 will increase the overlap between the illumination area and the collection area; therefore, it may increase the Raman signals collected. Theoretical modeling (Monte Carlo simulation) and experimental testing will be combined to optimize the distance (i.e. the thickness of the window) between the probe 116 and the tissue surface 170.

The filter adapter 120 will consist of two identical pre-aligned filter holders 125 and 129, preferably from OZ Optics Ltd. (Carp, ON, Canada). The OZ Optics filter holder 125 consists of a collimating lens 124 to collimate the light beam from the illumination fiber 130 before incident on the BP filter 122 and a refocusing lens 123 to focus the filtered beam onto the illumination fiber 132 in the fiber bundle assembly 110. The filter holder 129 consists of a collimating lens 128 to collimate the light from the collection fibers 180 before incident on the notch filter 126 and a refocusing lens 127 to focus the filtered light into the round-to-parabolic linear array 140. The single fiber 132 and fiber bundle 180 are connected to the filter adapter 120 by SMA connectors. A holder will attach the filter adapter 120 to the bronchoscope 116.

The fiber bundle 110 consists of 58 100- μm fibers. It is packed into circular shape and terminated with an SMA connector to the filter adapter 122. At the spectrometer 152 end, the 58 fibers 40 are aligned along a curve 154 formed by laser drilling of a stainless steel cylinder piece, the shape of which corresponds directly to the horizontal displacement shown in Figure 4 and expressed as a parabolic curve in Eq. (1) above. This curve serves to correct for image

aberration of the spectrograph 52 to achieve better spectral resolution and higher S/N ratio in a fashion similar to the skin Raman probe described in the '948 patent.

The probing fiber bundle assembly 110, the filter adapter 120, the laser light source 150 and illumination fiber 130, 32, the round-to-parabolic linear array 140, and the spectrometer 152 are integrated to form the endoscopic Raman probe system 100.

While a preferred embodiment of the present invention is shown and described, it is envisioned that those skilled in the art may devise various modifications of the present invention without departing from the spirit and scope of the appended claims.